Helicopter Trim with Flap-Lag-Torsion and Stall by an Optimized Controller

David A. Peters,* Mnaouar Chouchane,† and Mark Fulton†
Georgia Institute of Technology, Atlanta, Georgia 30332

An autopilot is applied to helicopter rotor flap-lag-torsion equations to obtain the control settings for a trimmed flight condition. The rotor aerodynamic description includes a state-space dynamic stall model for lift and for pitching moments. Thus, the rotor is trimmed for flight conditions in which significant stall and torsional deformations are present. The autopilot is extended to Q-bladed rotors by a series of time-delay terms. As a result, the optimum gains and time constants depend upon the number of blades as well as upon the torsional stiffness.

Nomenclature

a = slope of the airfoil lift curve, (/rad)
b = blade semichord, $c/2$
$\bar{b}$ = nondimensionalized blade semichord, b/R
C_D = drag force coefficient, $D/\pi R^2\rho\Omega^2R^2$
C_L = hub roll moment coefficient, $L/\pi R^2\rho\Omega^2R^2$
$\bar{C}_L$ = normalized roll moment coefficient, $C_L/\sigma a$
C_M = pitch moment coefficient, $M/\pi R^3\rho\Omega^2R^2$
$\bar{C}_M$ = normalized pitch moment coefficient, $C_M/\sigma a$
C_{ml} = linear pitching moment coefficient
C_T = blade thrust coefficient, $T/\pi R^2\rho\Omega^2R^2$
$\bar{C}_T$ = normalized blade thrust coefficient, $C_L/\sigma a$
C_z = lift coefficient, $\bar{L}/U^2$
C_{zl} = static lift coefficient in the linear region
C_{zs} = static lift coefficient
C_ζ = Rayleigh damping coefficient
c = blade chord, m
$\bar{c}$ = nondimensionalized blade chord, c/R
D = airfoil profile drag per unit length, N/m
d = stall damping parameter
E = Young's modulus, N/m^2
e = phase shift parameter
$\bar{e}$ = aerodynamic center offset divided by chord
e_A = distance between shear center and center of airfoil area
F_x, F_y = aerodynamic forces per unit length in the deformed blade, N/m
$\bar{f}$ = flat plate drag area divided by πR^2
I_x = blade flapping inertia, kg-m^2
$I_{y'}, I_{z'}$ = cross-sectional area moment of inertia, m^4
I_{ij}^{mn}, J_{jk}^{mn} = Galerkin integrals defined in Ref. 16
J = torsional rigidity constant, m^4
K_0, K_1 = collective and cyclic gains, rad^{-1}
K_β = stiffness of flap root spring, Nm/rad
K_ϕ = stiffness of torsional root spring, Nm/rad
K_ζ = stiffness of lag root spring, Nm/rad
k = inverse of reduced velocity, $\Omega b/V = \bar{b}/(\bar{r}+\mu\sin\psi)$
$\bar{k}$ = average value of k, $\bar{b}/\bar{r}$
k_m = blade cross-sectional radius of gyration, m
L = aerodynamic lift per unit length, N/m
$\bar{L}$ = lift per unit length divided by $\rho\Omega^2R^3$
L_α, L_N = circulatory and noncirculatory lift, respectively, N/m
L_u, L_v, L_w = generalized aerodynamic forces per unit length in the undeformed reference system, N/m^2
M_ϕ = generalized aerodynamic moment per unit length, mN/m
m = mass per unit length of the blade, kg/m
p = dimensionless rotating flapping frequency, $\sqrt{1+K_\beta/\Omega^2I_x}$
Q = number of blades
R = blade length, m
r = distance from hub center, m
$\bar{r}$ = r/R
s = apparent mass coefficient
t = time, s
U = blade airfoil velocity with respect to air, m/s
U_x = velocity component of the blade airfoil parallel to the chord, m/s
U_y = velocity component of the blade airfoil perpendicular to the chord, m/s
u, v, w = elastic deformations in x, y, z directions, respectively, m
$\bar{u}, \bar{v}, \bar{w}$ = nondimensional elastic deformations, $(u, v, w)/R$
V_i = induced downwash velocity, m/s
$V(\bar{r}), W(\bar{r})$ = comparison functions for bending
x, y, z = inertial coordinate system for undeformed blade, m
x', y', z' = inertial coordinate system for the deformed blade
α = airfoil angle of attack, rad
β = rigid blade flap angle, rad
γ = Lock number
$\bar{\Gamma}$ = nondimensional circulation, $\bar{L}/U$
Γ_m = normalized pitching moment, C_{m2}/U
ϵ = scaling parameter in the ordering scheme, $=0.1$
$\dot{\epsilon}$ = rate of rotation of the airfoil with respect to air mass taken with respect to nondimensional time, rad/s
ζ = rigid blade lag angle, rad
θ = blade pitch angle, rad
$\theta_0, \theta_s, \theta_c$ = collective and cyclic pitch angles, rad
λ = time delay parameter
Λ_1 = nondimensional parameter, $EI_{z'}/m\Omega^2R^4$
Λ_2 = nondimensional parameter, $EI_{y'}/m\Omega^2R^4$
Λ_3 = nondimensional parameter, $G/m\Omega^2$
Λ_4 = nondimensional radial stiffness, $AE/m\Omega^2R^2$
μ = advance ratio
ρ = air density, kg/m^3
σ = rotor solidity, $Qc/\pi r$

Received June 7, 1989; revision received Feb. 5, 1990.

*Professor, School of Aerospace Engineering. Associate Fellow AIAA.
†Research Assistant, School of Aerospace Engineering.

τ_0, τ_1 = time constants
ϕ = torsional deflection, rad
ψ = rotor azimuth angle, $= \Omega t$
Ω = rotor blade angular velocity, rad/s

Superscripts

$\cdot$ $= \partial/\partial t(\ )$
$'$ $= \partial/\partial x(\ )$
$+$ $= \partial/\partial x(\ ) = 1/R\ \mathrm{d}(\ )/\mathrm{d}x$
$*$ $= \partial/\partial\psi(\ ) = 1/\Omega\ \mathrm{d}(\ )/\mathrm{d}t$

Subscripts

x, y = x and y components
1, 2 = unstalled, stalled contributions

Introduction

COMPUTATION of the vibrations and stability of rotary-wing aircraft in forward flight requires finding a periodic solution to a set of nonlinear, time-varying, partial differential equations. This, in itself, can be a formidable task because the periodic solution may be very lightly damped or even unstable. Therefore, conventional time integration is not always satisfactory. However, whether the periodic solution is stable or unstable, the computation is made even more difficult by the fact that the equations contain unknown trim parameters (such as pilot control settings, airframe orientation angles, etc.) that must be chosen such that the final periodic solution satisfies the trim-equilibrium equations of a given flight condition. Thus, the rotary-wing analyst is faced with the solution of nonlinear equations with integral constraints on the solution. The solution of this constrained problem stands as one of the most difficult obstacles to analysis of rotary-wing aircraft with many degrees of freedom.

Currently, there are many proposed solution methodologies for this problem. Each has its strengths and weaknesses. For the time-domain solution, there are three general categories of methods. First, there are time-marching algorithms (i.e., numerical integration), including conventional methods as well as finite elements in time.[1] Second, there are harmonic-balance techniques of various types.[2] Third, there are transition-matrix methods including convolution[3] and periodic shooting.[4] For the solution of the trim constraints, there are also several alternatives. First, there is Newton-Raphson iteration on the control variables (which involves a complete periodic solution for each control perturbation). Second, there are closed-form force-balance equations that can be used as constraint equations to be solved in parallel with the other equations.[5] Third, there are autopilots that "fly" the rotor to trim during the time-marching towards a periodic solution.[6]

Once a periodic, trimmed equilibrium has been found, the dynamicist must find the dynamic behavior of perturbations away from this periodic orbit. This is often complicated by the fact that the aerodynamics models used in the equations either have hidden dynamic states or else have an infinite number of dynamic states (due to time delays, lift-deficiency functions, etc.). Furthermore, many of the trim methodologies (such as transition-matrix methods or periodic shooting) also require explicit knowledge of these states. Therefore, another challenge for the analyst is to develop aerodynamic theories that have explicit states. To this end, several researchers have investigated state-variable wake models,[7-9] and others have investigated finite-state lift models that include dynamic stall.[10-13]

In this paper, we explore trimming by the autopilot method. The autopilot method is not appropriate near blade stability boundaries. However, it is very efficient for well-damped rotors with many degrees of freedom and with complicated aerodynamics. In the past, however, its deficiency has been that a user would not know a priori what gains, time constants, and couplings to use. Those optimized in hover, for example, often failed in forward flight. One purpose of this paper is to improve those controllers. The rotor equations include elastic flap, lag, and torsion, and they include the dynamic stall model of Ref. 12 with several improvements. For example, the present work includes state variables that describe the unsteady pitching moments. The existing autopilot equations, although previously optimized for simple linear flapping, have never been applied successfully to flap-lag-torsion in forward flight with high thrust and significant stall. Therefore, we have reformulated the autopilot and reoptimized it for these more stringent conditions. This paper describes the results of this reformulation on rotor trimming. The work is an extension of that found in Ref. 14. The extensions to that work are 1) addition of torsional degree of freedom, 2) addition of elastic modes, 3) extension of lift model to include pitching moment, 4) improvement of lift model for better behavior at high angles of attack, 5) reformulation of autopilot to include more than one blade, 6) reformulation of autopilot couplings to include forward-flight terms, and 7) studies of adaptive autopilot gains. The second purpose of this paper is to examine the limits of trim with the improved controller.

Mathematical Model of Rotor

Structural Model

We present here the vertical and inplane bending equations and the torsion equation. The nondimensional form is obtained by division of both sides of the dimensional form of each equation by $m\Omega^2 R$. Terms including blade precone are not considered here. The derivation and a more extensive discussion related to these equations can be found in Ref. 15. Only terms of order ϵ and ϵ^3 are retained in the nondimensional flap equation:

$$-(\tau\bar{w}^{+})^{+} + (\Lambda_1 - \Lambda_2)(\theta + \phi)\bar{v}^{+\,+\,+} + [\Lambda_2 + (\Lambda_1 - \Lambda_2)(\theta + \phi)^2]\bar{w}^{+\,+\,+\,+} + \ddot{\bar{w}} = \bar{L}_w \tag{1}$$

In the lag equation, terms of order ϵ^2 and ϵ^4 are retained:

$$-(\tau\bar{v}^{+})^{+} + [\Lambda_1 + (\Lambda_2 - \Lambda_1)(\theta + \phi)^2]\bar{v}^{+\,+\,+} + (\Lambda_1 - \Lambda_2)(\theta + \phi)\bar{w}^{+\,+\,+\,+} + 2\dot{\bar{u}} + \ddot{\bar{v}} - \bar{v} = \bar{L}_v \tag{2}$$

where

$$\dot{\bar{u}} = -\int_0^x \bar{w}^{+}\dot{\bar{w}}^{+}\,\mathrm{d}\bar{x} \tag{3}$$

The torsion equation is written in a nondimensional form with terms of order (ϵ^4)

$$-\Lambda_3 J\phi^{+\,+} + \bar{e}(\overline{xw}^{+} + \ddot{\bar{w}}) - \bar{e}_A\bar{w}^{+\,+}\Lambda_4\left(\bar{u}^{+} + \frac{\bar{w}^{+2}}{2}\right) = \bar{M}_\phi \tag{4}$$

where τ is the nondimensional tension expressed as

$$\tau(1,\epsilon^2) = \frac{1 - x^2}{2} + \int_{\bar{x}}^{1}(2\dot{\bar{v}} + \bar{u} - \ddot{\bar{u}} + \bar{L}_u)\,\mathrm{d}\bar{x} \tag{5}$$

The generalized aerodynamic forces per unit length in the inertial reference system L_v and L_w are expressed in terms of L_x and L_y, which are the aerodynamic forces per unit length in the deformed blade coordinates. They are expressed in a nondimensional form as follows:

$$\bar{L}_v = -[\bar{L}_x\cos(\theta + \phi) + \bar{L}_y\sin(\theta + \phi)] \tag{6}$$

$$\bar{L}_w = [-\bar{L}_x\sin(\theta + \phi) + \bar{L}_y\cos(\theta + \phi)] \tag{7}$$

The preceding equations have been compared in Ref. 15 with other work related to blade equations. When the equa-

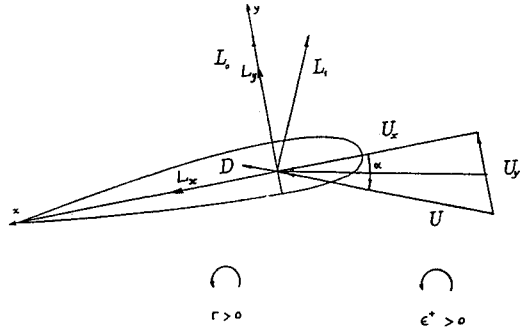

Fig. 1 Aerodynamic forces in the deformed blade coordinate system.

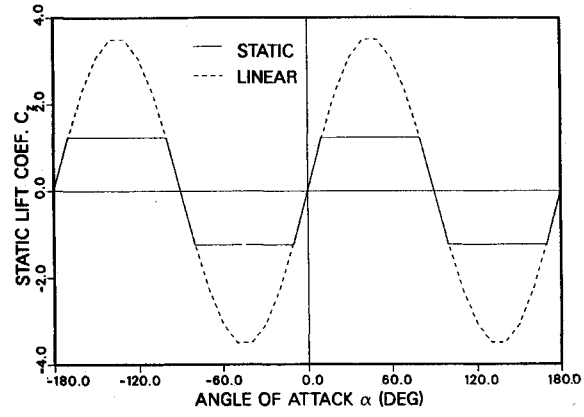

Fig. 2 Static and linear lift coefficients vs angle of attack.

tions are written to the higher order, they include all the terms of the equations derived by other authors and more. This is due to the assumptions and the method used in the derivation, in addition to the scaling procedure.

Unified Lift Model

The unified lift model extends the ONERA model to include plunge, unsteady freestream, and large angles of attack. In the modification, a distinction is made between angle of attack due to pitch motion and angle of attack due to plunging motion. Furthermore, the unified model separates the apparent mass lift from the circulatory lift. Thus, we have for the components of lift normal to the chord L_y and along the chord L_x (see Fig. 1),

$$\bar{L}_y = \bar{L}_0 + U_x(\bar{\Gamma}_1 + \bar{\Gamma}_2) \tag{8}$$

$$\bar{L}_x = -U_y(\bar{\Gamma}_1 + \bar{\Gamma}_2) \tag{9}$$

where U_x and U_y are the components of the flow along the chord and normal to the chord, respectively, and where L_0 is the apparent mass lift

$$\bar{L}_0 = \bar{b}_s \dot{U}_y \tag{10}$$

The unified model has the same structure as the Greenberg and Theodorsen theories at small angles of attack. A complete discussion of the refinement that led to the unified model is presented in Ref. 12. The simplified version, in which reversed flow is approximated and higher-order terms in $\bar{\Gamma}_2$ equation are neglected, is

$$\bar{k}\dot{\bar{\Gamma}}_1 + \lambda\bar{\Gamma}_1 = \lambda a U_y + \delta\bar{b}\dot{\epsilon} \tag{11}$$

$$\bar{k}^2\ddot{\bar{\Gamma}}_2 + 2dwk\dot{\bar{\Gamma}}_2 + w^2(1+d^2)\bar{\Gamma}_2 = -w^2(1+d^2) \times \left[U_x\Delta C_z + e\bar{k}\left(\dot{U}_x\Delta C_z + \frac{\partial \Delta C_z}{\partial \alpha}\dot{U}_y\right)\right] \tag{12}$$

where U_x and U_y are normal and chordwise airflow relative to the airfoil, and $\bar{k}$ is an average of the reduced frequency of the freestream. The coefficients δ, w, d, and e are dynamic-stall coefficients evaluated at the instantaneous angle of attack, $\alpha = \tan^{-1}(U_y/U_x)$, and $\dot{\epsilon}$ is the rotation of the airfoil with respect to the air mass. This model is used in the present research work to determine the aerodynamic forces applied on the blade. Although it does not present a perfect representation of the aerodynamic environment in stall regime, it has been shown to give good agreement with experiments and it is certainly more reasonable than the linear, quasisteady theory currently used in most stability analyses. Three-dimensional aerodynamic effects are included through the wake model and through a tip-loss factor. The former accounts for forward-flight effects and the latter for tip effects.

Stall Coefficients

In the preceding equations, the total circulation density Γ is expressed as a sum of two components Γ_1 and Γ_2; Γ_1 is the circulation density associated with a linear model. However, Γ_2 is the deviation of the circulation from the linear value due to stall. The model is expressed by differential equations that depend on ΔC_z, which is the difference between the potential-flow static lift coefficient ($C_{zl} = a\sin\alpha$) and the actual stalled lift coefficient C_{zs}.

The coefficients λ, a, s, δ, d, w, and e depend on the angle of attack only. In Table 1, we present, for illustrative purposes, the numerical values of these coefficients determined by wind tunnel tests and parameter identification for an OA212 airfoil. In this table, u is the unit step function. It is equal to unity for a positive argument and zero otherwise.

The static lift curve for a typical airfoil is presented in Fig. 2. The lift coefficient is linear between -10 and 10 deg. For large angles, the magnitude shows a deviation from linearity. The static coefficient extrapolated from the linear region is C_{zl}. The actual static lift is C_{zs}. In the unified lift model in

Table 1 Identified coefficients of stall equations

Parameter	Numerical value	Physical description
λ	0.2	Time delay parameter
s	$5\pi/180$	Apparent mass quantity
$\bar{\delta}$	$\left(\frac{\partial C_z}{\partial \alpha} - \frac{4\pi}{180}\right)(1 + 1.43\Delta C_z)$	Relates lift coefficient to the pitch rate
w	$0.10 + 0.023(\lvert\alpha\rvert - 13\text{ deg})u(\lvert\alpha\rvert - 13\text{ deg})$ $\lvert\alpha\rvert < 21.7$ 0.3 $\lvert\alpha\rvert > 21.7$	Damping factor
d	$0.105/w$	Stall natural frequency
ϵ	$2 - 5.1\tan^{-1}[1.21(\lvert\alpha\rvert - 13\text{ deg})]u(\lvert\alpha\rvert - 13\text{ deg})$	Relates lift coefficient to the pitch rate

Ref. 12, the linear component of the circulation with reversed flow is expressed as

$$\Gamma_l = aU \sin\alpha \cos\alpha \tag{13}$$

where, for the OA212 airfoil, $a = 7.1$. (It is $>2\pi$ due to Mach number.)

Aerodynamic Pitching Moment Model

The pitching moment per unit length about the aerodynamic center, positive nose up, is expressed in Ref. 11 as

$$M_\phi = \frac{1}{2}\rho 2b^2\left[V^2C_{ml} + V^2C_{m2} + c_1 b\frac{\partial}{\partial t}(V\theta + \dot{h}) + c_2 bV\dot{\theta} + c_3 b^2\ddot{\theta}\right] \tag{14}$$

In the preceding equation, C_{ml} is the linear static moment coefficient, C_{m2} is the nonlinear component of the pitching moment due to stall, θ is the pitch angle, and h is the plunge velocity positive downward. The coefficients c_1, c_2, c_3 are empirical coefficients that depend on the Mach number and that have been found to have the following expressions for the OA212 airfoil:

$$c_1 = -\frac{\pi}{4}(1 + 1.4M^2) \tag{15}$$

$$c_2 = c_1 \tag{16}$$

$$c_3 = -\frac{3\pi}{16}\{-1.26 - 1.53 \arctan[15(M - 0.7)]\} \tag{17}$$

The effect of the airfoil geometry on the pitching moment due to unstalled flow is included through the C_{ml} coefficient only.

The curves of the actual static moment coefficient C_{ms} and its linear counterpart C_{ml} for an OA212 airfoil are presented in Fig. 3. It is important to mention that this curve is accurate for small positive angles of attack ($0 \le \alpha \le 26$ deg). The extension of the curve for other angles is approximate. This extension was guided by typical airfoil test data. For large angles of attack and in the reversed flow regime, the goal is to use a well-behaved approximation of the static coefficients since the angle of attack of any blade section more often falls in the range of small or moderate angles ($0 \le \alpha \le 25$ deg).

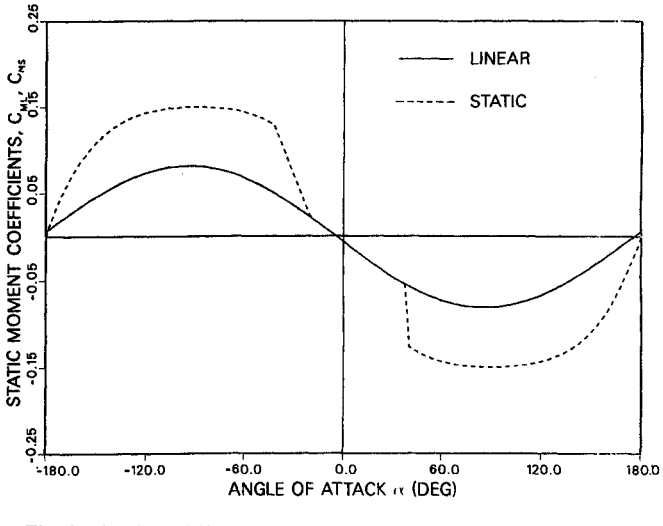

Fig. 3 Static and linear moment coefficient vs angle of attack.

The nonlinear moment coefficient C_{m2} is computed from the following expression where $\Gamma_{m2} = UC_{m2}$:

$$\bar{k}^2\ddot{\Gamma}_{m2} + a\bar{k}\dot{\Gamma}_{m2} + r\Gamma_{m2} = -rU\Delta C_m - E\bar{k}\dot{U}_y \tag{18}$$

The coefficients of the Γ_{m2} equation were found to have common forms for a variety of airfoils. Each coefficient depends on the geometry of the airfoil and ΔC_z, the difference between the actual static lift coefficient and its linear counterpart. These coefficients have the following expressions:

$$r = (r_0 + r_2\Delta C_z^2) \tag{19}$$

$$a = a_0 + a_2\Delta C_z^2 \tag{20}$$

$$E = E_2\Delta C_z^2 \tag{21}$$

It can be noted that the Γ_{m2} coefficient is equal to zero when the flow is not stalled. This is due to the fact that ΔC_m and E are both equal to zero for this case.

Now, Eq. (14) needs to be reviewed to incorporate in it the correct definition of angles used in the present paper. First, the torsional angle ϕ should be added to the pitch angle θ due to the pitch controller. Second, in Greenberg theory the fourth term of Eq. (14) must include all rotations of the airfoil with respect to air mass, even if they are not caused by blade pitch. Hence, $\dot{\theta}$ should be replaced by $\dot{\epsilon}$ in Eq. (14), which is the rate of rotation with respect to air mass. The resultant model is then specifically formulated for rotor blade analysis. This model, excluding the first two terms, agrees with the aerodynamic model used in Ref. 15.

The torsion, Eq. (4), requires the nondimensional form of the M_ϕ expression. This expression is obtained by division of the equation for M_ϕ by $m\Omega^2R^2$ to obtain

$$\bar{M}_\phi = \frac{1}{6}\frac{\gamma\bar{c}}{a}[U^2C_{ml} + U\Gamma_{m2} + c_1\bar{b}\dot{U}_y + c_2\bar{b}U\dot{\epsilon} + c_3\bar{b}^2(\ddot{\theta} + \ddot{\phi})] \tag{22}$$

Since the aeroelastic equations used in the blade analysis of the present work should have ordered terms, the terms of the above equation need to be scaled. Table 2 summarizes the order of each term and its components based on actual helicopter data. It follows from this ordering scheme that the last term of Eq. (22) is of higher order. This term is the apparent-mass moment. Hence, this term can be omitted when the lower-order equation is used.

When this model is used in conjunction with the elastic equations, an integration of M_ϕ along the blade span needs to be performed. To facilitate this integration, the third and fourth terms of Eq. (22) can be expressed explicitly as func-

Table 2 Scaling of the terms of the moment equation

Parameter	Value or expression	Assumed order
U	$U \approx U_x(1, \epsilon^2)$	1
C_{ml}	$-0.08 \rightarrow 0.08$	ϵ
C_{m2}		1
c_1	$c_1 \approx -\pi/4$	1
c_2	$c_2 \approx c_1$	1
c_3	$c_3 \approx -3\pi/16$	1
$\bar{b}$		1
$\dot{\theta}$		ϵ
$\gamma\bar{c}/6a$	≈ 0.02	ϵ^2
U^2C_{ml}		ϵ^2
U^2C_{m2}		ϵ^2
$c_1\bar{b}\dot{U}_y$		ϵ^2
$c_2\dot{U}\epsilon$		ϵ^2
$c_3\bar{b}^2\ddot{\alpha}$		ϵ^4

tions of the radial position. Thus, each term has a unique expression along the blade span, and a simple integration can be performed analytically or numerically. However, for the first two terms of Eq. (22), the integration procedure is more complex since C_{ml} and Γ_{m2} have no algebraic expressions. Instead, C_{ml} and Γ_{m2} can only be evaluated at some chosen sections. Computing Γ_{m2} at many sections would introduce many more second-order differential equations. Any increase of the number of differential equations to be solved obviously leads to a slower computational speed. Thus, C_{ml} and Γ_{m2} must be discretized at no more than 5–10 positions, and then interpolation functions give values for intermediate stations.

Autopilot Equations

Trim Formulation

Any flight vehicle should be able to maintain equilibrium during steady flight conditions. This means that the resultant forces and moments on the aircraft are equal to zero. In a conventional fixed-wing aircraft, external aerodynamic control surfaces (such as ailerons, elevators, and rudders) perform these functions.

In a helicopter, trim is performed by variation of blade angle as a function of the azimuthal position of the blade so that rolling and pitching of the aircraft is avoided. This is accomplished through pilot-controlled inputs of collective pitch (θ_0) and cyclic pitch (θ_s, θ_c). The pitch mechanism produces the pitch setting for a helicopter trimmed condition that is expressed as follows:

$$\theta = \theta_0 + \theta_s \sin\psi + \theta_c \cos\psi \tag{23}$$

In the trimmed condition, the rotor is maintained at a fixed thrust coefficient C_T in forward flight. Thus, the trim procedure requires the knowledge of the helicopter control settings as the azimuth angle varies, depending on the flight condition.

There are two trim conditions commonly used for numerical trimming purposes: moment trim and propulsive trim. In moment trim, the rotor shaft maintains a preset angular position, and the blade pitch is varied by using cycling pitch to cancel pitch and roll moments. This is typical of wind tunnel testing. In propulsive trim, rotor shaft tilt is added to overcome fuselage drag that is more typical of free flight. In either case, collective pitch is used to balance rotor weight or to give a desired thrust. In this paper, we present results for moment trim only.

Automatic Feedback Controls

One way of trimming the helicopter is to use an automatic feedback system that would trim the helicopter automatically as the rotor equations are integrated in time. Here, the control settings are assumed unknown. Hence, they are calculated simultaneously along with the generalized coordinates of the blade equations. One possible form of the autopilot equations is derived in Ref. 6. These equations can be expressed in either of the following two forms:

$$\begin{bmatrix} \tau_0 & 0 & 0 \\ 0 & \tau_1 & 0 \\ 0 & 0 & \tau_1 \end{bmatrix} \begin{Bmatrix} \ddot{\theta}_0 \\ \ddot{\theta}_s \\ \ddot{\theta}_c \end{Bmatrix} + \begin{Bmatrix} \dot{\theta}_0 \\ \dot{\theta}_s \\ \dot{\theta}_c \end{Bmatrix} = \begin{bmatrix} K_0 & 0 & 0 \\ 0 & K_1 & 0 \\ 0 & 0 & K_1 \end{bmatrix}$$

$$\times \begin{bmatrix} \dfrac{8p^2}{\gamma} & 0 & 0 \\ 0 & \dfrac{8(p^2-1)}{\gamma} & -1 \\ 0 & 1 & \dfrac{8(p^2-1)}{\gamma} \end{bmatrix} \begin{Bmatrix} \Delta\beta_0 \\ \Delta\beta_s \\ \Delta\beta_c \end{Bmatrix} \tag{24}$$

$$\begin{bmatrix} \tau_0 & 0 & 0 \\ 0 & \tau_1 & 0 \\ 0 & 0 & \tau_1 \end{bmatrix} \begin{Bmatrix} \ddot{\theta}_0 \\ \ddot{\theta}_s \\ \ddot{\theta}_c \end{Bmatrix} + \begin{Bmatrix} \dot{\theta}_0 \\ \dot{\theta}_s \\ \dot{\theta}_c \end{Bmatrix} = \begin{bmatrix} K_0 & 0 & 0 \\ 0 & K_1 & 0 \\ 0 & 0 & K_1 \end{bmatrix}$$

$$\times \begin{bmatrix} \dfrac{6}{\sigma a} & 0 & 0 \\ 0 & \dfrac{-16}{\sigma a} & \dfrac{2\gamma}{\sigma a(p^2-1)} \\ 0 & \dfrac{-2\gamma}{\sigma a(p^2-1)} & \dfrac{-16}{\sigma a} \end{bmatrix} \begin{Bmatrix} \Delta C_T \\ \Delta C_L \\ \Delta C_M \end{Bmatrix} \tag{25}$$

where

$$\Delta\bar{C}_T = \bar{C}_T - \frac{4}{3}\frac{p^2}{\gamma}\beta \tag{26}$$

$$\Delta\bar{C}_L = \bar{C}_L + \frac{p^2-1}{\gamma}\beta \sin\psi \tag{27}$$

$$\Delta\bar{C}_M = \bar{C}_M + \frac{p^2-1}{\gamma}\beta \cos\psi \tag{28}$$

$$\Delta\beta_0 = \frac{3}{4}\frac{\gamma}{p^2}\bar{C}_T - \beta \tag{29}$$

$$\Delta\beta_s = \frac{-2\gamma}{(p2-1)}\bar{C}_L - 2\beta \sin\psi \tag{30}$$

$$\Delta\beta_c = \frac{-2\gamma}{(p2-1)}\bar{C}_M - 2\beta \cos\psi \tag{31}$$

These Δ quantities represent the errors between the desired values of thrust, roll moment, or pitch moment (or, alternatively, of coning and tip-path tilt) and the instantaneous values of these quantities from the rotor mathematical model. Thus, they are the errors that must be set to zero to achieve a desired trim condition. For moment trim, $\bar{C}_T$ is set at the desired thrust coefficient, and $\bar{C}_L$ and $\bar{C}_M$ are set to zero. This automatic feedback system is used to provide control to the helicopter for numerical purposes. It adjusts the pitch of the blade to maintain thrust, roll moment, and pitching moment. The parameters K_0 and K_1 are controller gains. The parameters τ_0 and τ_1 are time constants. The controller reaches steady state when the errors are zero.

Application of the preceding equations has shown unsatisfactory performance for high advance ratios or high lifting conditions. One explanation for this deficiency can be linked to the hover assumption inherent in the above gains and couplings. A more accurate formulation of the above couplings can be obtained from the control responses in Ref. 2. These response derivatives are verified, in that same reference, to give accurate results at low to moderate advance ratios. By using these response derivatives to formulate the couplings of the feedback controller, the model is expected to expand the range of accurate trimming performance to higher advance ratios.

In general, the static derivatives between controls and loads can be written in a matrix form as follows

$$\begin{Bmatrix} dC_T \\ dC_L \\ dC_M \end{Bmatrix} = [A] \begin{Bmatrix} d\theta_0 \\ d\theta_s \\ d\theta_c \end{Bmatrix} \tag{32}$$

In hover, $\mu = 0$, we have

$$[A_0] = \begin{bmatrix} \frac{1}{6} & 0 & 0 \\ 0 & -\frac{C^2}{16(1+C^2)} & \frac{-C}{16(1+C^2)} \\ 0 & \frac{C}{16(1+C^2)} & -\frac{C^2}{16(1+C^2)} \end{bmatrix} \tag{33}$$

and where $C = [8(p^2-1)/\gamma]$. These are the couplings implicit in Eqs. (24) and (25).

The more accurate form of these response derivatives in forward flight is given in Ref. 2 and is

$$[A_\mu] = \begin{bmatrix} \frac{1}{6}\left(1+\frac{3}{2}\mu^2\right) & \frac{2}{9}\mu & 0 \\ -\frac{C}{6}\frac{\mu}{1+C^2}\left\{C-\frac{\gamma}{16p^2}\right\} & -\frac{C}{16(1+C^2)}\left\{C\left(1+\frac{3}{2}\mu^2\right)-\frac{2}{9}\mu^2\frac{\gamma}{p^2}\right\} & -\frac{C}{16(1+C^2)} \\ \frac{C}{6}\frac{\mu}{1+C^2}\left\{1+C\frac{\gamma}{16p^2}\right\} & \frac{C}{16(1+C^2)}\left\{(1+2\mu^2)+\frac{2}{9}\mu^2 C\frac{\gamma}{p^2}\right\} & -\frac{C^2}{16(1+C^2)}\left(1+\frac{\mu^2}{2}\right) \end{bmatrix} \tag{34}$$

These equations are derived in Ref. 2 based on a harmonic balance of rigid-body blade flapping in forward flight. The assumptions of that derivation are quasisteady aerodynamics and no reversed flow. Hence, from the above matrix, a feedback system can be formed in a similar manner as described previously:

$$\begin{bmatrix} \tau_0 & 0 & 0 \\ 0 & \tau_1 & 0 \\ 0 & 0 & \tau_1 \end{bmatrix}\begin{Bmatrix} \ddot{\theta}_0 \\ \ddot{\theta}_s \\ \ddot{\theta}_c \end{Bmatrix} + \begin{Bmatrix} \dot{\theta}_0 \\ \dot{\theta}_s \\ \dot{\theta}_c \end{Bmatrix} = \begin{bmatrix} K_0 & 0 & 0 \\ 0 & K_1 & 0 \\ 0 & 0 & K_1 \end{bmatrix}$$

$$\times [A_\mu]^{-1}\begin{bmatrix} \frac{C_T}{\sigma a} - \frac{4}{3}\frac{p^2}{\gamma}\beta \\ \frac{C_L}{\sigma a} + \frac{p^2-1}{\gamma}\beta\sin\psi \\ \frac{C_M}{\sigma a} + \frac{p^2-1}{\gamma}\beta\cos\psi \end{bmatrix} \tag{35}$$

The preceding system of equations, Eq. (35), reduces to Eq. (25) in hover (i.e., $\mu = 0$).

Optimized Controller

Previous studies to optimize the controller have resulted in a variety of combinations of gains and time constants, each resulting in a "minimum" settling time of about 5-8 rotor revolutions. In those studies, Refs. 6 and 14, settling time was minimized subject to constraints on stability and limits on the oscillations of the final control positions due to higher harmonic input signals from β. To understand these results, it is useful to write equations for a general controller of the type specified in Eq. (35):

$$\begin{bmatrix} \tau_i & \\ & \ddots \end{bmatrix}\begin{Bmatrix} \ddot{\theta}_i \\ \vdots \end{Bmatrix} + \begin{Bmatrix} \dot{\theta}_i \\ \vdots \end{Bmatrix} = \begin{bmatrix} K_i & \\ & \ddots \end{bmatrix}[A]^{-1}\begin{Bmatrix} \bar{C}_D - C_A \\ \vdots \end{Bmatrix} \tag{36}$$

where τ_i are time constants (to filter out oscillatory inputs), θ_i are the controls, K_i are gains, $[A]$ is a matrix of control couplings, C_A are computed trim variables, and $\bar{C}_D$ are the desired values of C_A. A crucial step in understanding these equations is to understand that C_A is related to the controls in the following way:

$$\{C_A\} = \{C_A\}_0 + [B]\{\theta_i\} \tag{37}$$

Thus, the closed-loop control equations become

$$\begin{bmatrix} \tau_i & \\ & \ddots \end{bmatrix}\begin{Bmatrix} \ddot{\theta}_i \\ \vdots \end{Bmatrix} + \begin{Bmatrix} \dot{\theta}_i \\ \vdots \end{Bmatrix} + \begin{bmatrix} K_i & \\ & \ddots \end{bmatrix}[A]^{-1}[B]\begin{Bmatrix} \ddot{\theta}_i \\ \vdots \end{Bmatrix}$$

$$= \begin{bmatrix} K_i & \\ & \ddots \end{bmatrix}[A]^{-1}\begin{Bmatrix} \bar{C}_D - C_{A0} \\ \vdots \end{Bmatrix} \tag{38}$$

In past studies (and this present one), the controller is designed such that $[A]$ is taken to be as close to $[B]^{-1}$ as possible. When this is done exactly, the homogeneous equations for each control become uncoupled,

$$\tau_i\ddot{\theta}_i + \dot{\theta}_i + K_i\theta_i = 0 \tag{39}$$

This gives a natural frequency $\omega_n = \sqrt{K_i/\tau_i}$, a damping ratio $\zeta = 1/(2\sqrt{K_i\tau_i})$, and a settling time $t_s = 1.46/K_i$ (revolutions) for $\zeta < 1$. It is clear that an optimum controller would have infinite gain. However, there are some higher-order blade dynamics implicit in the B matrix that are not included in the approximation of Eq. (37) nor in the quasisteady $[A]$ couplings. Thus, large K can drive the system unstable. Therefore, optimum designs have tended first to increase K to near the stability boundary and then to choose τ large enough to filter out oscillatory response but small enough to keep ω_n around 0.25 to 0.33 (3 to 4 rotor revolutions per controller cycle).

Nevertheless, despite these fairly successful efforts, oscillations in final control settings have not been completely satisfactory due to the fact that only a single blade is modeled, which gives large 2/rev oscillations in C_T (θ_0) and large 1/rev oscillations in C_L and C_M (θ_s and θ_c). To solve this problem, we have, by taking information from past time history as "other" blades, modified the controller to assume that Q blades are present. Thus, rather than feeding back $C_A(\bar{t})$, we feed back

$$\bar{C}_A(\bar{t}) = \frac{C_A(\bar{t}) + C_A\left(\bar{t}-\frac{2\pi}{Q}\right) + C_A\left(\bar{t}-2\frac{2\pi}{Q}\right) + \cdots + C_A\left(\bar{t}-\frac{Q-1}{Q}2\pi\right)}{Q} \tag{40}$$

This essentially filters out from C_A all harmonics not integer multiples of Q. However, it also introduces additional time delays into the system. For example, for $Q = 2$, if we use the Padé approximate to the time delay, we obtain for the homogeneous equation

$$\frac{\pi}{2}\dddot{\theta}_i + \left(\tau + \frac{\pi}{2}\right)\ddot{\theta}i + \dot{\theta} + K\theta_i = 0 \tag{41}$$

Thus, there is a higher-order $\dddot{\theta}$ term (negligible for small values of ω_n) and there is also an added $\pi/2$ on the $\ddot{\theta}$ term that gives an implicit τ. In general, for Q blades, the equivalent total τ on the $\ddot{\theta}$ term is

$$\tau_{eq} = \frac{Q-1}{Q}\pi + \tau \tag{42}$$

In the limit as Q goes to infinity, we define the limits of Eq. (40):

$$\bar{C}_A = \frac{1}{2\pi}\int_{\bar{t}-2\pi}^{\bar{t}} C_A(t)\,dt \tag{43}$$

Thus, for $\tau = 0$ and $Q = \infty$, we have $\tau_{eq} = \pi$, which is about the optimum found from previous work. Thus, for $Q = \infty$, the $\ddot{\theta}$ term could be removed from our controller, giving

$$\begin{Bmatrix} \vdots \\ \dot{\theta}_i \\ \vdots \end{Bmatrix} = \begin{bmatrix} \diagdown & & \\ & K_i & \\ & & \diagdown \end{bmatrix} [A]^{-1} \begin{Bmatrix} \vdots \\ \bar{C}_D - C_A \\ \vdots \end{Bmatrix} \tag{44}$$

Figure 4 shows the settling time for such a controller as a function of equal gains, $K_0 = K_1$. (Discontinuities occur when the settling time moves off of a given peak to a new peak.) Thus, the optimum gain is about 0.15. However, as we shall see, when additional unmodeled dynamics enter the problem, K must be reduced for stability. In the following work, we use the $Q = 2$ controller so that the $\ddot{\theta}$ term must be retained, with a small added time constant τ. We have found that the $Q = 2$ controller filters out all unwanted control oscillations, is easy to program, and allows more flexibility in the choice of τ_{eq}.

Figure 4 also illustrates one of the difficulties in optimizing for settling time. Because settling time (to a given value of decay) can be discontinuous, many optimization routines have difficulty in finding the minimum value. We have found the optimum by a combination of optimization codes (such as OPT and CONMIN), by graphical techniques, and by optimization with more continuous cost functions such as integrals of error over time.

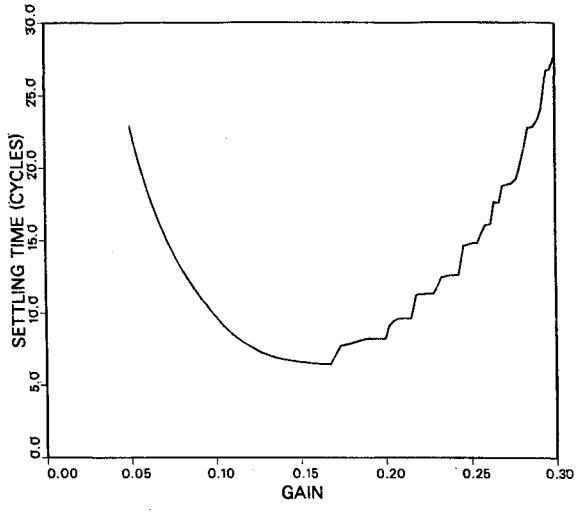

Fig. 4 Settling time vs gain.

Results

Solution Method

In this section, a Ritz-Galerkin method is applied to the elastic blade model, Eqs. (1), (2), and (4), which then are combined with Eqs. (35). The aerodynamic circulations are expressed by Eqs. (11), (12), and (18). Only lower-order terms of these equations are considered in the following analyses to reduce complexity. This allows the investigation of the general trends without going into cumbersome computation. The coupling of the structural, aerodynamic, and control models is quite easy since all are state-space models described by ordinary differential equations. Thus, the control states are easily substituted into the aerodynamic and structural models at each time step. Similarly, the circulations are placed directly into the structural equations, Eqs. (40–50). Finally, the thrust and root moments (required for the controller) are evaluated directly from Eqs. (26–28) that depend only on β (the first flapping mode). Thus, an advantage of these state-space models is the ease of implementation.

The flap, lag, and torsion equations presented above are nonlinear partial differential equations with variable coefficients. A Ritz-Galerkin method is often used to obtain an approximate solution for the blade equations. The method consists of assuming a solution of the problem in the form of a series composed of a linear combination of admissible functions, W_j for flap bending, V_r for lag bending, and ϕ_l for torsional deflections, multiplied by the time-dependent functions (generalized coordinates), q_j for flap, p_r for lag, and r_l for torsion, respectively,

$$\bar{w} = \sum_{j=1}^{n} W_j(\bar{x})q_j(\psi) \tag{45}$$

$$\bar{v} = \sum_{r=1}^{n} V_r(\bar{x})p_r(\psi) \tag{46}$$

$$\phi = \sum_{l=1}^{n} \Phi_l(\bar{x})r_l(\psi) \tag{47}$$

The application of the above procedure transforms the flap, lag, and torsion Eqs. (1), (2), and (4) to ordinary differential equations. The coefficients of the equations have integral forms that can be determined after selecting comparison functions. These coefficients are presented in Ref. 16. The resultant equations are

Flap equation:

$$\sum_{j=1}^{n} I_{ij}^{6}\ddot{q}_j + \sum_{j=1}^{n}(I_{ij}^{10} + \Lambda_2 I_{ij}^{8} + \bar{K}_\beta B_{ij}^{1})q_j = \frac{\gamma}{6a}\sum_{l=1}^{m}(\bar{\Gamma}_{1l} + \bar{\Gamma}_{2l})(\mu \sin\psi\, I_{il}^{4} + I_{il}^{5}) \tag{48}$$

Lag equation:

$$\sum_{j=1}^{n} J_{ij}^{6}\ddot{p}_j + \sum_{j=1}^{n}(J_{ij}^{10} - J_{ij}^{6} + \Lambda_1 J_{ij}^{8} + \bar{K}_\zeta B_{ij}^{1})p_j - 2\sum_{j=1}^{n}\sum_{k=1}^{n} J_{ijk}^{13}\dot{q}_k q_j + (\Lambda_1 - \Lambda_2)(\theta + \phi)\sum_{j=1}^{n} J_{ij}^{8}q_j = -\frac{\gamma}{6a}\sum_{j=1}^{n}\sum_{l=1}^{m}(\bar{\Gamma}_{1l} + \bar{\Gamma}_{2l})(J_{ijl}^{12}\mu\cos\psi q_j + J_{ijl}^{11}\dot{q}_j + \bar{V}_i J_{il}^{4}) + C_D\frac{\gamma}{6a}(J_i^3 + 2\mu\sin\psi J_i^2 + \mu^2\sin^2\psi J_i^1) \tag{49}$$

Torsion equation:

$$\sum_{j=1}^{n} \bar{k}_m^2 I_{ij}^{16} \ddot{r}_j - \frac{1}{6}\frac{\gamma\bar{c}^2}{a} c_1 (I_{ij}^{17} + \mu \sin\psi I_{ij}^{16}) \dot{r}_j$$

$$+ \sum_{j=1}^{n} (\bar{K}_\phi B_{ij}^2 + \Lambda_3 \bar{J} I_{ij}^{18} - \frac{1}{12}\frac{\gamma\bar{c}^2}{a} c_1 \mu \cos\psi I_{ij}^{16}) r_j$$

$$= \frac{1}{6}\frac{\gamma\bar{c}}{a}\left\{ \sum_{l=1}^{m} (C_{mLl} + C_{m2l})[I_{il}^{24} + 2\mu \sin\psi I_{il}^{23} + (\mu \sin\psi)^2 I_{il}^{22}] \right.$$

$$+ c_1 \bar{b}[(2\dot{\theta} + v_c \sin\psi) I_i^{15} + \mu(2\dot{\theta} \sin\psi + \theta \cos\psi) I_i^{14}]$$

$$\left. + c_1 \bar{b} \sum_{j=1}^{n} [-\mu \cos\psi I_{ij}^{20} \dot{q}_j + (I_{ij}^{21} + 2\mu \sin\psi I_{ij}^{20}) q_j - I_{ij}^{19} \ddot{q}_j] \right\} \tag{50}$$

After selection of n comparison functions for each equation, it is possible to compute the coefficients of the preceding equations. This results in $3n$ linear differential equations to be solved for the generalized coordinate in time domain.

Before moving to the aerodynamic equations, it is convenient to discuss the selection of comparison functions required for the above equations. The results obtained in Figs. 5–11 are based on the rigid blade assumption. This approximation is used in the early stages of this work to validate the aeroelastic model and to trace its efficiency and drawbacks in less complicated cases. Results in Figs. 12–15 are for an elastic blade model with torsion. In either case, we use the so-called K-polynomials of Ref. 15 as comparison functions. These satisfy the natural boundary conditions at the blade tip.

Table 3 gives the common parameters used in the cases discussed in this section. These parameters are selected from current helicopter data and used for illustration purposes. Note that the lift-curve slope is greater than 2π due to compressibility. The drag coefficient is assumed constant in the work presented here. The authors have already reviewed a few nonlinear drag models and implemented them for simple problems. In future work, we intend to include a nonlinear drag model and to include a variable C_D based on the stall assumption. The study conducted so far concentrates on the effect of stall on lift but not on drag. The controller gains and time constants were chosen from a formal optimization procedure applied to linear, rigid-blade flapping equations at $\mu = 0.3$.

Table 3 Baseline parameters

Parameter	Numerical value	Physical description
γ	6.63	Lock number
a	6.461	Lift-curve slope
C_D	0.01	Drag coefficient
Λ_1	0.014	$EI_y/m\Omega^2R^4$
Λ_2	0.002	$EI_x/m\Omega^2R^4$
$\bar{b}$	0.05	b/R
p	1.03	Flap frequency
f	0.01	Flat plate drag
σ	0.1	Solidity
K_β	0.0203	Stiffness of flap root
K_ζ	0.02083	Stiffness of lag root
C_ζ	0.025	Damping coefficient
τ_0	2.94	Time constant
τ_1	0.31	Time constant
K_0	0.27	Gain
K_1	0.18	Gain

Steady-State Response

The determination of the steady-state response of rotor blades is necessary for the prediction of loads and vibrations. The differential equations describing the blade response are integrated in time until all the transients have died out and a periodic and trimmed response is obtained. A case is considered to be trimmed when the control settings θ_0, θ_s, and θ_c reach stable positions. The control angles are considered to be converged when they reach a value within ± 0.5 deg of their final value in a limited number of cycles. Usually, the controller will reach convergence with 6 to 12 revolutions. The trim procedure suppresses the first harmonic oscillations of controls through the $Q = 2$ time delay.

The flap and lag are initially set to zero. The initial values of the control settings, on the other hand, are computed using approximate trim equations. This method allows a reasonable initial guess of the controllers that reduces the convergence time.

Results have been obtained for a variety of advance ratios and thrust coefficients. The results are given for the final revolution. Though the majority of cases converge in less than 10 cycles, it takes longer for those conditions close to the convergence boundaries of the controller.

Effect of Advance Ratio

Advance ratio is the normalized freestream velocity with respect to the blade tip speed. At high advance ratios, the retreating blade encounters large angles of attack. This causes a region of the rotor to enter the stall regime. We now will present rotor response for four moderate to high values of advance ratio at a constant thrust coefficient $C_T = 0.01$. A single C_T is chosen so that it illustrates the response at the trim boundaries. The rate of convergence becomes slower as the advance ratio increases. Figure 5 gives time histories of the control angle θ_0 at several advance ratios. Ideally, the control settings should reach a steady state. As advance ratio increases to 0.38, once-per-revolution oscillations begin to have an increasing effect on the controllers. The amplitude of this once-per-revolution response becomes larger with μ, and the convergence rate diminishes with μ. At advance ratios above 0.38, these effects take on a more significant role until there is no convergence.

The reason for this deterioration of convergence is that the increase of dynamic stall is introducing a once-per-revolution lift input that is not "expected" by the A_μ coupling (which is based on quasisteady theory). Thus, the controller is unable to cope with this change. Furthermore, the stall is making it impossible (from a physical standpoint) to obtain enough lift to trim. The loss of lift can be seen in Fig. 6, which gives the contribution of a single blade section to the total lift. The figure shows a hysteresis loop, which is typical of dynamic response. Large negative angles of attack can occur at the most inboard element due to reversed flow. This element,

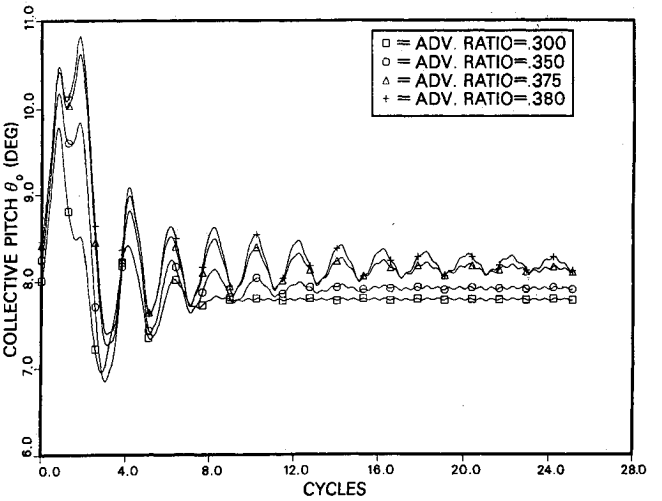

Fig. 5 Collective pitch vs cycles of rotation, $C_T = 0.01$.

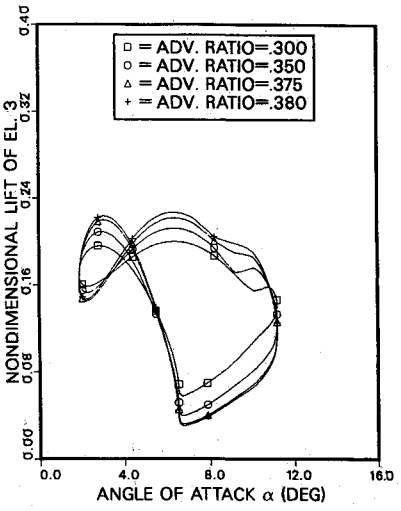

Fig. 6 Nondimensional lift of element 3 vs angle of attack, $C_T = 0.01$.

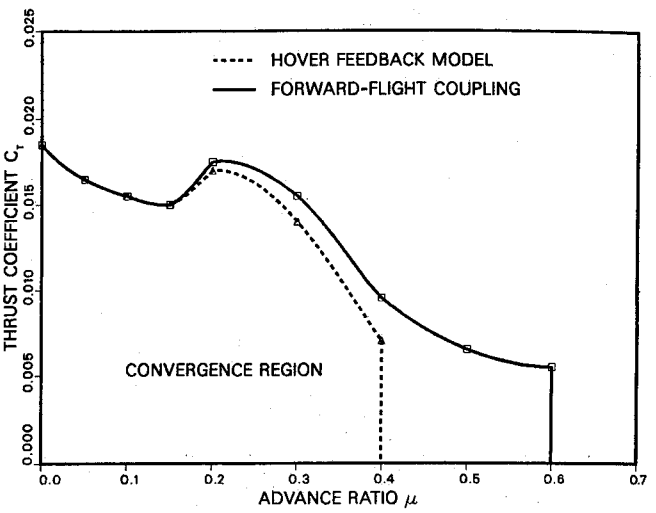

Fig. 8 Trim boundaries for two control cases.

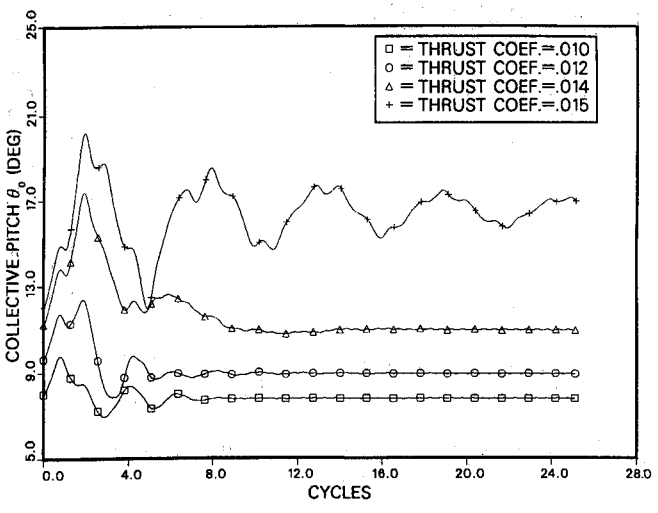

Fig. 7 Collective pitch vs cycles of rotation, $\mu = 0.30$.

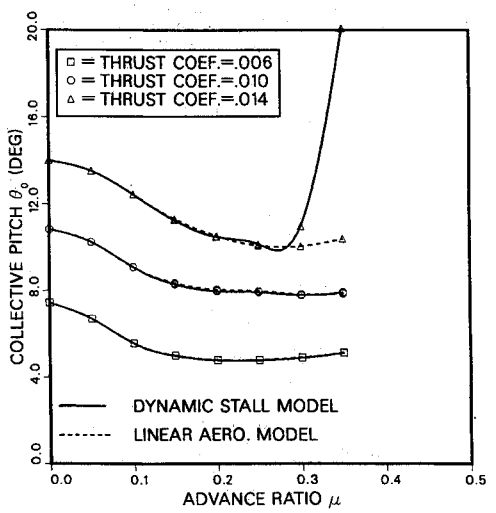

Fig. 9 Collective pitch vs advance ratio.

however, has an average positive angle of attack through one revolution.

Effect of Thrust on Trim

Rotor response may be effected considerably by stall either when the advance ratio increases or when the gross weight is increased for the same rotor. Figure 7 illustrates the time history of the control response for a constant advance ratio, $\mu = 0.3$, and for various values of the thrust coefficient. As the thrust coefficient increases, the convergence becomes slower, and the effect of the once-per-revolution component becomes more significant. At a thrust coefficient of $C_T = 0.015$, the convergence is very slow compared to the other cases. Figure 8 shows the limits of C_T and μ for which the rotor can be trimmed. The dashed curve is with the hover control couplings, $[A_0]^{-1}$, and the solid line is for the more accurate couplings, $[A_\mu]^{-1}$. The main effect of improved couplings is to shift the trim limits from $\mu = 0.4$ to $\mu = 0.6$. There is much less change on the C_T boundary. This implies that the C_T boundary is a physical limitation to trim rather than a numerical limit.

In Figs. 9–11, the control settings are plotted as functions of the advance ratio for various thrust levels for both the complete dynamic stall model and for a linear aerodynamic model. The linear model is similar to the complete one except that the nonlinear aerodynamic component is ignored. Thus, it is a linear aerodynamic model in which the linearity continues even beyond the critical angle of attack. The collective pitch θ_0 decreases to a minimum due to induced flow effects and then increases slowly as the advance ratio reaches higher values. This variation is in conjunction with the typical variation of the power required with cruise speed. On the other hand, the cyclic pitch is zero at hover, $\mu = 0$. This is because of the symmetry of the blade coning at hover. The longitudinal cyclic pitch θ_s increases in magnitude with advance ratio to account for the loss of freestream velocity on the retreating blade. The lateral cyclic pitch θ_c is associated with the trim of aerodynamic coupling due to coning. Thus, it increases until it reaches an approximately stationary value.

For low values of thrust coefficients, both models predict the same control settings. At high loadings, such as $C_T = 0.014$, the controls have higher values with stall modeled. In particular, the longitudinal cyclic pitch increases more significantly at the beginning of the stall regime. This is because the loss of lift is more pronounced in the neighborhood of $\psi = 270$ deg. For $\mu = 0.35$, the response is close to trim but not fully trimmed. This is in agreement with Fig. 8, which shows $C_T = 0.014$, $\mu = 0.35$ to be slightly over the trim boundary.

Effect of Torsion on Trim

When the torsional degree of freedom and elastic modes are included in the aeroelastic model, the controller with the previous gains and time constants ($\tau_0 = 2.94$, $\tau_1 = 0.31$, $K_0 = 0.27$,

$K_1 = 0.18$) fails to attain a trimmed condition for torsional frequencies lower than 8/rev. This failure occurs for any choice of advance ratio μ and thrust coefficient C_T. To understand this failure, recall that torsional deflections enter into the blade dynamics through a variable torsional angle (for an elastic blade), which is added to the blade pitch. High torsional frequency (>8/rev) corresponds to a blade with high torsional rigidity for which the effect of torsion on lift is not important. A blade that is torsionally soft, however, causes the torsional defections to have a more significant effect on the controller. An examination of those cases that failed to trim revealed that the controller was oscillating in an unstable manner. Since the system stability depends directly on the cyclic gains, these gains were lowered until a stable situation was obtained (i.e., $K_1 = 0.05$). The new choice of gains allows the controller to trim successfully for torsional frequencies as low as 5/rev. However, for torsional frequencies lower than 5/rev, numerical experiments with gains did not bring any significant improvement to trim. Thus, an adaptive $[A] = [B]^{-1}$ may be required for those conditions.

The collective and cyclic pitch produced by the low-gain controller are shown in Figs. 12–14. The torsional angle is shown in Fig. 15. Several observations can be drawn from these figures. First, the variation of the torsional deflection agrees with the physical expectation. Both the average and the

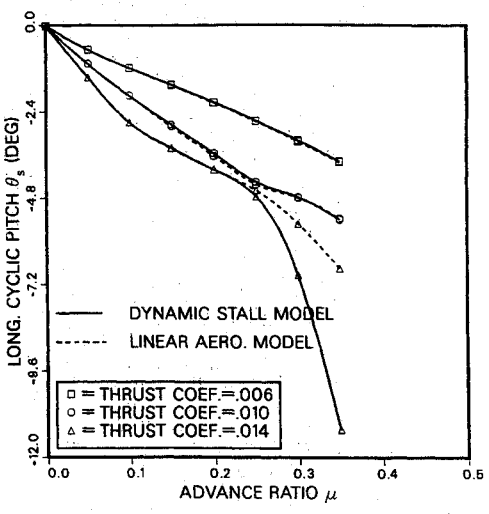

Fig. 10 Longitudinal cyclic pitch vs advance ratio.

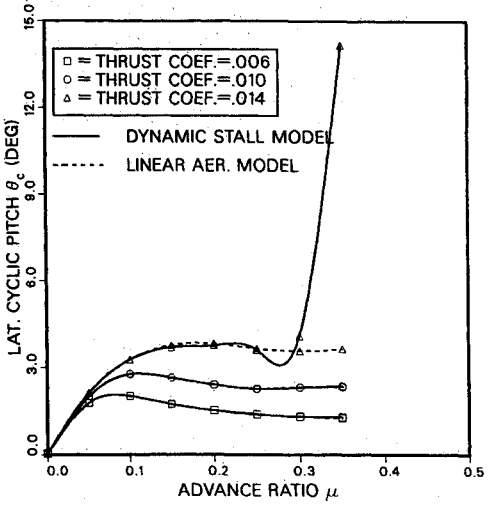

Fig. 11 Lateral cyclic pitch vs advance ratio.

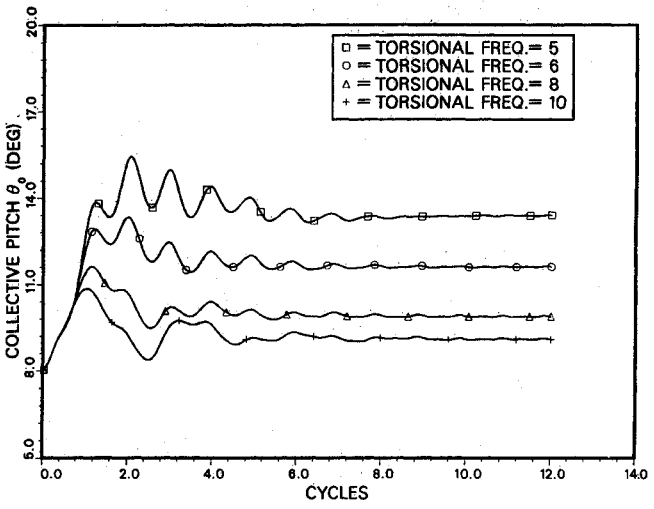

Fig. 12 Collective pitch vs cycles of rotation, $C_T = 0.01$ and $\mu = 0.30$.

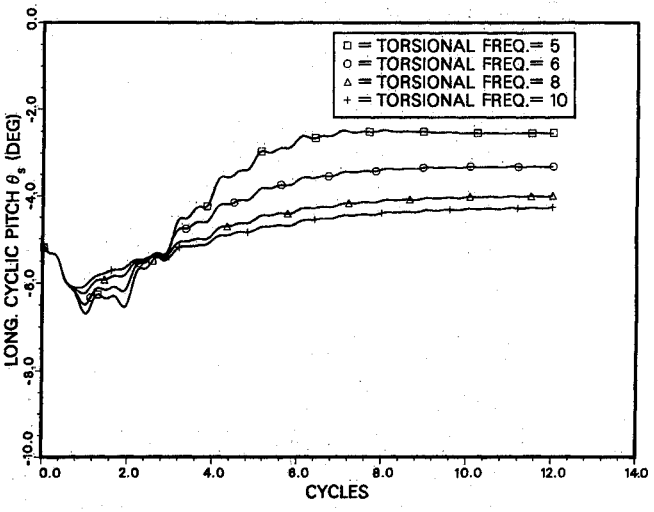

Fig. 13 Longitudinal cyclic pitch vs cycles of rotation, $C_T = 0.01$ and $\mu = 0.30$.

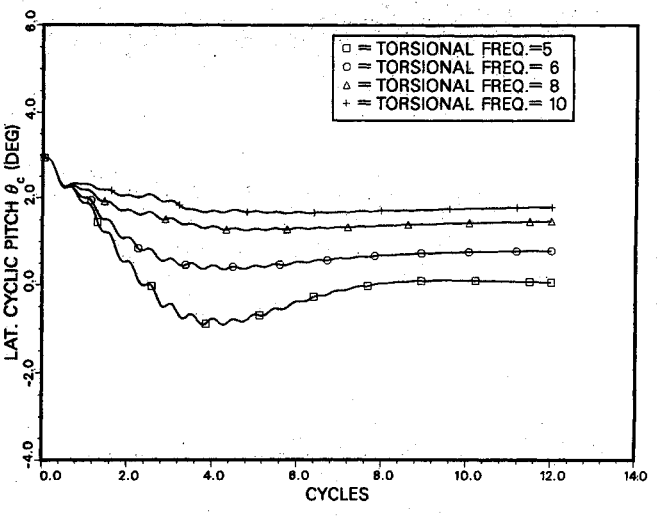

Fig. 14 Lateral cyclic pitch vs cycles of rotation, $C_T = 0.01$ and $\mu = 0.30$.

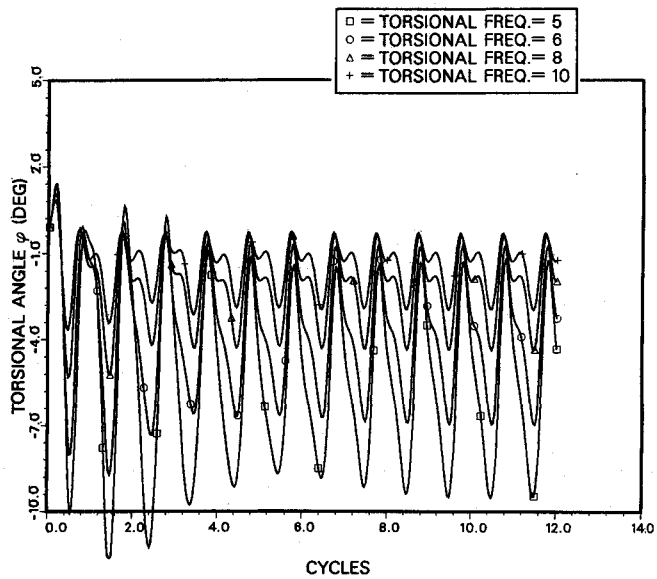

Fig. 15 Torsional deflection vs cycles of rotation, $C_T = 0.01$ and $\mu = 0.30$.

oscillatory amplitude of torsional deflections increase as the torsional frequency decreases. Since this average is negative, the collective pitch must increase to maintain the desired lift (see Fig. 12). Similarly, the longitudinal and lateral pitch angles decrease for lower frequencies because torsional deflection oscillations are dominated by once-per-rev oscillations.

Further, numerical experiments and theoretical observations (not given here) confirm that a trimmed condition for low torsional frequencies cannot be achieved by a simple adjustment of the gains and time constants, since some approximations are inherent in the autopilot couplings.[16] One approximation is the neglect of the torsional deflection in the angle-of-attack expression used during the derivation of the coupling matrix. Thus, for soft torsion where these deflections play a more important role, the coupling matrix may have to be modified to include the effect of torsion. Although approximate theoretical methods could be used to add effect of torsion to the coupling matrix, an adaptive numerical method may be necessary for the general case.

Conclusions

A more general rotor autopilot has been developed. It is formulated in a general way so as to be applicable to any number of trim variables (although in this paper we consider only three). To write such a controller, one needs information on the errors in each trim condition ($\bar{C}_D - C_A$), a matrix $[A]$ that gives approximate relationships between each control θ_i and each trim variable $\partial A_j/\partial\theta_i$, and a set of gains K_i (to be found from trial-and-error or optimization). In general, if $[A]$ is well modeled, all K can be made equal to 1/(period of rotor revolution). If only a finite number of blades are used, then $\ddot{\theta}$ terms are also required having an equivalent coefficient of $\pi/(Q\Omega^2)$.

Results of helicopter trim with this autopilot have been obtained for an elastic-blade rotor model and a state-space stall model. The presence of these structural and aerodynamic models is very compatible with the autopilot algorithm, and the equations are easily coupled. Trim was obtained over a wide range of flight conditions even when $[A]$ was chosen based on linear, rigid-blade dynamics. However, for torsional frequencies less than 5/rev, a more accurate $[A]$ is necessary. We propose that such an $[A]$ be found from an adaptive controller.

Acknowledgments

The development of the optimized controller was sponsored by Interdisciplinary Research Division, NASA Langley Research Center, Grant NAG-1-710, Howard Adelman, technical monitor. The development of the state-space stall model and the flap-lag-torsion modeling were performed in the Georgia Institute of Technology Center of Excellence for Rotary-Wing Aircraft Technology with funding from the Army Research Office, Robert Singleton, technical monitor.

References

[1]Panda, B., and Chopra I., "Flap-Lag-Torsion Stability in Forward Flight," *Journal of the American Helicopter Society,* Vol. 30, No. 4, 1985, pp. 30–39.

[2]Peters, D. A., and Ormiston, R., "Flapping Response Characteristics of Hingless Rotor Blades by a Generalized Harmonic Balance Method," NASA TN D7856, Feb. 1975.

[3]Friedmann, P. P., and Kottapalli, S.-B.-R., "Coupled Flap-Lag-Torsional Dynamics of Hingeless Rotor Blades in Forward Flight," *Journal of the American Helicopter Society,* Vol. 27, No. 4, 1982, pp. 28–36.

[4]Peters, D. A., and Izadpanah, A., "Helicopter Trim by Periodic Shooting with Newton-Raphson Iteration," Paper 81-23, *Proceedings of the 37th Annual National Forum of the American Helicopter Society,* Alexandria, VA, May 1981.

[5]Eipe, A., "Effect of Some Structural Parameters on Elastic Rotor Loads by an Iterative Harmonic Balance," Ph.D. Thesis, Dept. of Mechanical Engineering, Washington Univ., St. Louis, MO, Dec. 1979.

[6]Peters, D. A., Kim, B. S., and Chen, H.-S., "Calculation of Trim Settings of a Helicopter Rotor by an Optimized Automatic Controller," *Journal of Guidance, Control, and Dynamics,* Vol. 7, No. 1, 1984, pp. 85–91.

[7]Friedmann, P. P., and Venkatesan, C., "Finite State Modeling of Unsteady Aerodynamics and Its Application to a Rotor Dynamic Problem," Paper 72, *Proceedings of the 11th European Rotorcraft Forum,* London, Sept. 10–13, 1985.

[8]Johnson, W., "General Time-Domain Unsteady Aerodynamic of Wings," *Proceedings of the 25th Aircraft Symposium of Japan Society for Aeronautical and Space Sciences,* Tokyo, Dec. 14–16, 1987.

[9]Peters, D. A., and He, C. J., "Comparison of Measured Induced Velocities With Results From a Closed-Form Finite State Wake Model in Forward Flight," *Proceedings of the 45th Annual National Forum of the American Helicopter Society,* Boston, MA, May 22–24, 1989.

[10]Elliott, A. S., "Calculation of the Steady Periodic and Gust Response of a Hingless Rotor Helicopter Using Two-Dimensional Time Domain Unsteady Aerodynamics," Ph.D Thesis, Univ. of Maryland, College Park, MD, 1987.

[11]Tran, C. T., and Petot, D., "Semi-Empirical Model for the Dynamic Stall of Airfoils in View of the Application to the Calculation of Responses of a Helicopter Blade in Forward Flight," *Vertica,* Vol. 5, No. 1, 1981, pp. 35–53.

[12]Peters, D. A., "Toward a Unified Lift Model for Use in Rotor Blade Stability Analysis," *Journal of the American Helicopter Society,* Vol. 30, No. 3, 1985, pp. 32–42.

[13]Petot, D., and Dat, R., "Unsteady Aerodynamic Loads on an Oscillating Airfoil with Unsteady Stall," *Proceedings of the Helicopter Research Workshop,* Florida Atlantic Univ., Boca Raton, FL, Nov. 1987.

[14]Peters, D. and Chouchane, M., "Effect of Dynamic Stall on Helicopter Trim and Flap-Lag Response," *Journal of Fluids and Structures,* Vol. 1, No. 1, 1987, pp. 299–318.

[15]Karunamoorthy, S. N., and Peters, D. A., "Use of Hierarchical Elastic Blade Equations and Automatic Trim For Rotor Response," *Vertica,* Vol. 11, No. 2, 1987, pp. 233–248.

[16]Chouchane, M., "Application of a Dynamic Stall Model to Rotor Trim and Aeroelastic Response," Ph.D. Thesis, Georgia Inst. of Technology, Atlanta, GA, Aug. 1989.